ADVANCED ENGINEERING MATERIALS

DOI: 10.1002/adem.201600669

Extraction of Flow Behavior and Hall–Petch Parameters Using a Nanoindentation Multiple Sharp Tip Approach**

By *Alexander Leitner*, *Verena Maier-Kiener* and *Daniel Kiener**

An appealing idea to material scientists is to characterize the mechanical behavior of materials with minimal experimental effort while guaranteeing highly reliable results. Nanoindentation is a candidate technique to reach this objective. Though it is already a standard method to extract hardness and Young's modulus, the technique is not yet fully exploited. The authors demonstrate on the example of Ni and W, with microstructures ranging from single crystalline to nanocrystalline dimensions, how Hall–Petch parameters and flow curves can be extracted by using four pyramidal tips with varying apex angle. Applying appropriate definitions of indentation stress and strain and considering the indentation size effect, the obtained values coincidence well with literature values determined by uniaxial tests.

1. Introduction

The mechanical characterization of materials by simple hardness measurements attracts attention in engineering disciplines since decades.[1,2] Nowadays, nanoindentation provides the opportunity to extract a variety of mechanical properties on the nano- or micro-scale and, thus, is of great interest especially for limited volumes of interest. Nanostructured materials, often only produced in bench-scale, are in the focus of researchers due to their outstanding strength and functionality.[3] Their mechanical characterization is of prime interest, which may be among the governing reasons why the number of publications per year on nanoindentation steadily increases since more than 20 years. The determination of hardness H and Young's modulus E following the analysis introduced by Oliver and Pharr[4] is common practice by now, but also more sophisticated techniques seize the material research community. By way of example, obtaining stress–strain curves from nanoindentation which are comparable to uniaxial flow curves is of great interest and has been extensively investigated in recent years.[5–12] One major asset is that the stress state with a high hydrostatic part allows testing materials with poor ductility, where mechanical and rate-dependent behavior would not be accessible in conventional uniaxial tests. Furthermore, it enables studying the hardening behavior of single crystals.[13] Still the technique has not yet asserted as a standard testing method. By reviewing the existing literature, one realizes that there are still several uncertainties. In a strict sense, discrepancy starts at the definition of hardness per se, which is imprecisely defined as the resistance of a material to the penetration of a harder material. The analysis of conventional hardness tests compared to instrumented indentation may yield to significantly differing values and shall be part of the focus of the present study.[14] Furthermore, the introduced stress-state is multiaxial and therefore it is not self-evident to define a representative strain ε_r and representative stress σ_r corresponding to uniaxial tests. Basic findings are that the stress strongly correlates with hardness and that strain is dependent

[*] *Dr. D. Kiener, A. Leitner*
Department of Materials Physics, Montanuniversität Leoben, and Erich-Schmid-Institute for Materials Science, Austrian Academy of Sciences, Jahnstraße 12, A-8700 Leoben, Austria
E-mail: daniel.kiener@unileoben.ac.at
Dr. V. Maier-Kiener
Department of Physical Metallurgy and Materials Testing, Montanuniversität Leoben, Roseggerstraße 12, A-8700 Leoben, Austria

[**] *Funding of the Styrian and the Tyrolean Provincial Government, represented by Steirische Wirtschaftsförderungsgesellschaft mbH and Standortagentur Tirol, within the framework of the COMET Funding Programme (837900, MPPE A7.19) is appreciated. Further parts of this work were also funded by the Austrian Science Fund (FWF) via the project P25325-N20. All Ni samples were generously provided by DI Thomas Leitner and Prof. Reinhard Pippan (ESI Leoben). (Supporting Information is available online from Wiley Online Library or from the author).*
The copyright line of this paper was changed 16 March 2017 after initial publication.
This is an open access article under the terms of the Creative Commons Attribution License, which permits use, distribution and reproduction in any medium, provided the original work is properly cited.

at least on the geometry of the indenter tip.[15–17] For instance, in early works of Tabor cone-shaped tips with varying opening angles were used to perform macroscopic hardness tests.[16] A linear relation between H to σ_r was assumed, and linked by a constant called by constraint factor C^*. By comparing hardness to uniaxial stress–strain curves, C^* was determined to be close to 2.8. Additionally, this resulted in an empirical definition of a representative strain ε_r which was found to be dependent on the half apex angle of the used cones.[16,17] Surveyed, Tabor was likely not considering the additional influence of the materials parameter E/σ since the tested materials mild steel and copper show rather high values of around 800–1600 at which the C^* is rather insensitive.[18,19] Particularly, various FEM studies showed that C^* may strongly depend on this parameter.[9,10,18,20–22] Sophisticated dimensionless analysis gives an accurate approximation of C^*, but always requires knowledge of constitutive parameters such as yield strength, modulus, or hardening parameters a priori.[10–12,22] Once definitions for stress and strain are clarified, determination of stress–strain curves is a straight-forward procedure.

In the present work, we will conduct a detailed comparison of nanoindentation and Vickers microhardness tests, and follow Tabors work investigating the approach of determining stress–strain curves by nanoindentation using four sharp indenter tips with varying opening angle. To the best knowledge of the authors, this has never been conducted on metals so far. Four samples each of nickel and tungsten will be investigated where the specimen have microstructures reaching from single crystalline (SX) to nanocrystalline (NC) dimensions, ending up in a large interval of E/σ ratios and strongly different work-hardening behavior. In addition to their flow behavior, also Hall–Petch (HP) parameters will be extracted for both materials to examine whether hardness tests are actually suitable and comparable to parameters obtained from uniaxial tests. Finally, it will be demonstrated that the used analysis method leads to excellent flow curve data when applied to the tested materials compared to bulk literature data.

2. Experimental Section

2.1. Investigated Materials

Nickel and tungsten samples have been investigated in the present study. The high melting points ($T_{M,Ni} = 1\,455\,^{\circ}C$, $T_{M,W} = 3\,422\,^{\circ}C$[23]) will ensure that no microstructural changes occur at RT, particularly important for the NC and ultra-fine grained (UFG) specimen. Due to the face centered cubic (FCC) structure of Ni and body centered cubic (BCC) structure of W, possible influences of the crystal structure will be observable. Fine grained (FG) Ni, UFG Ni, and UFG W were fabricated by High Pressure Torsion (HPT), whereat former was annealed to coarsen the microstructure. Further details of fabrication and microstructure of UFG Ni and electrodeposited NC Ni can be obtained from the study by Leitner et al.[24] For details regarding CG W and FG W see the study of Maier et al.[25] Both, electrodeposited and HPT metals feature a high fraction of high angle grain boundaries (>65%),[26–28] thus no significant influence of the grain boundary character is expected. The orientations of SX samples were confirmed by electron backscatter diffraction (EBSD) where the Ni SX is oriented in (1 0 0) and W SX in (1 1 0). The mean grain size of the refined microstructures was either determined using EBSD (UFG and FG samples), X-Ray Diffraction (XRD) (Ni NC), or optical microscope (W CG, linear intercept method). The grain size determined by XRD has to be considered as a lower limit, since also sub-grain structures will be covered by this technique. Micrographs of all samples except the SX state are shown in Figure 1, where the images were obtained by a scanning electron microscope (SEM; LEO type 1525, Carl Zeiss GmbH, Germany) except of CG W, which was recorded using an optical microscope. All samples were mechanically and electrolytically polished in order to avoid any influences of surface preparation.

2.2. Nanoindentation Experiments

Indentation tests were conducted on a Nanoindenter G200 (Keysight Technologies, USA) with a continuous stiffness measurement (CSM) option. The frequency of the superimposed force was set to 45 Hz with a displacement amplitude of 2 nm. Hardness and Young's modulus were obtained by the standard analysis proposed by Oliver and Pharr.[4] CSM measurements allow to determine the mechanical properties continuously in dependence of indentation displacement. Thus, for isotropic materials, a horizontal profile of the Young's modulus over displacement is a feasible indicator for reliable measurements (see, e.g., Supplementary Figure S1). At least five indents were made with an indentation strain-rate of $0.05\,s^{-1}$ for each tip and material, and measurements were the thermal drift exceeded $0.1\,nm\,s^{-1}$ were discarded. Four 3-sided pyramidal diamond tips with varying face angle (FA) were tested on each material, details are given in Table 1. The Berkovich tip was manufactured by MicroStar, USA while the FA 80, FA 50, and Cube Corner tip were obtained from Synton MDP LTD, Nidau, Switzerland. The maximum displacement was set to be 2 500 nm, but for the FA 80 tip the device specific force limit of 500 mN was reached already at lower depths for materials with higher strengths. For perfect pyramidal tips the projected area depending on the contact depth is described by[4]:

$$A_c(h_c) = C_1 \cdot h_c^2, \tag{1}$$

where C_1 composes from the pyramidal geometry as

$$C_1 = 3 \cdot \sqrt{3} \cdot \tan^2(\alpha), \tag{2}$$

with α as the face angle of the pyramid. Hence, by calibration of the area function on an isotropic material such as fused quartz, one can assess C_1 experimentally and determine the actual face angle. In order to calculate ε_r of the respective tip,

 © 2016 The Authors. Published by WILEY-VCH Verlag GmbH & Co. KGaA, Weinheim

ADVANCED ENGINEERING MATERIALS

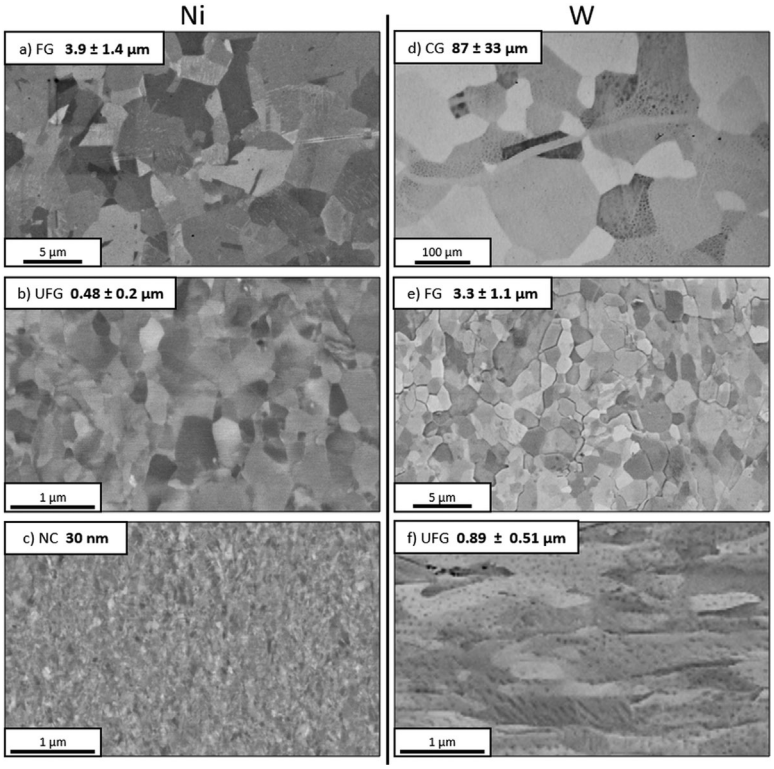

Fig. 1. SEM microstructure observations of the Ni (a–c) and W (e–f) sample. FG and UFG Ni (a and b) show HPT Ni samples in axial direction. (d) The microstructure of CG W was investigated with an optical microscope. (f) Shows UFG W in radial direction. Mean grain sizes are imprinted in the according images. Ni SX (1 0 0) and W SX (1 1 0) are not displayed.

the corresponding cone angle β will be needed which can be determined by

$$\tan(\beta) = \sqrt{\frac{C_1}{\pi}} \tag{3}$$

Table 1 shows the obtained data and compares the nominal strain predicted from the strain definition of Tabor[16] with the actual strain from calibrations, proofing that the tip shapes are very close to the ideal specifications. Furthermore, it is important to note that for materials exhibiting an indentation size effect (ISE) hardness should rather be determined at the same contact area than the same contact depth.[29,30] Table 1 shows the contact depths for each tip resulting in identical contact areas. Another approach is to determine the bulk hardness of the material following the analysis of Nix and Gao.[29] In their work, an extrapolation to the bulk hardness H_0 is possible if several data pairs of H and displacement h are experimentally measured:

$$\left(\frac{H}{H_0}\right)^2 = 1 + \frac{h^*}{h}, \tag{4}$$

where h^* is an internal length scale parameter which provides information on how pronounced the indentation size effect is. In the present study, the consequences of using either H at the same contact area or H_0 will be discussed.

2.3. Microhardness Testing

All microhardness measurements were performed on a BUEHLER Micromet 5100 using a diamond Vickers indenter. Depending on the material, loads F of either 200 or 500 gf were used to determine the Vickers hardness. Again at least five impressions were performed for each material. Diagonals (D) of residual impressions were measured with an optical microscope in order to calculate HV according to[1]:

$$HV = \frac{F \cdot 2 \cdot \sin\left(\frac{136^\circ}{2}\right)}{D^2} \tag{5}$$

2.4. Vickers Hardness versus Nanoindentation Hardness

Since hardness is dependent on the geometry of the used tip it is important to note that different hardness testing techniques are only restrictively comparable. Primary, tips have to be divided into two groups, self-similar (pyramidal tips, cones) and non-self-similar tips (e.g., spheres). In the present work, we will only focus on the self-similar type so that ε_r should not be influenced by the indentation depth. Secondly, for sharp tips the hardness value will be dependent on the tip opening angle. Therefore, if we want to compare conventional Vickers hardness testing with nanoindentation, we have to ensure that the representative cone has the same apex angle. For large indentation depths commonly reached

Table 1. Overview of used tips and their geometrical properties. Actual strain values compared to the nominal values imply that all tips are close to their specifications.

Tip	Face angle α	Representative cone angle β	Nominal strain ε_n	Actual strain ε_a	Mech. properties determined at
FA 80	80°	82.2°	2.74%	2.64%	250–350 nm
Berkovich	65.3°	70.3°	7.16%	7.16%	650–780 nm
FA 50	50°	56.9°	13.04%	12.62%	1190–1430 nm
Cube Corner	35.3°	42.3°	21.98%	21.65%	2000–2400 nm
Vickers	68° (4-sided)	70.3	7.16%	–	After unloading

in Vickers hardness testing imperfect tip shapes at low penetration depths can be neglected. This is not the case for nanoindentation and thereby the reason why three-sided pyramids are used. Three faces converging at one point will, for geometric reasons, necessarily give a sharp tip, while four faces will likely result in an edge instead. However, the proportions of a Berkovich tip were chosen in a way that it has the equal representative cone compared to a Vickers tip.

We would like to point out, that obtained hardness values can still not be directly compared, even though these values are sometimes mixed up in literature. The discrepancy results from two main aspects:

1) *Used contact area:* Vickers hardness refers to the load normalized by the real area in contact while in nanoindentation hardness load is divided by the projected area. However, this issue can simply be compensated by using D^2 instead of $D^2/\sin(\alpha)$ for the hardness calculation, resulting in a constant coefficient of 1.08 to convert the real contact area to the projected contact area in the case of Vickers and Berkovich tips.
2) *Consideration of real contact depth:* Vickers hardness is calculated from the size of the residual impression, while nanoindentation obtains the projected area in contact at maximum load. Particularly for materials with low Young's modulus and high hardness, such as fused quartz, this aspect may lead to a vast underestimation of microhardness. Unlike point (1), it is not possible to correct the hardness directly for Vickers measurements, since the stiffness of the material has to be known. In this work, we will always refer to the hardness definition of nanoindentation. Vickers values will be corrected by the stiffness obtained from nanoindentation measurements.

Another aspect to consider is the well-known indentation size effect for materials with a coarse microstructure, resulting from geometrically necessary dislocations and thereby introduced large strain gradients, especially at low indentation depths.[29] This can be accounted for by obtaining H_0 from Equation 4.

2.5. Stress and Strain Definitions for Hardness Testing

Beside different definitions of hardness per se, the conversion to a stress value is controversially discussed, too. In general, a linear relationship between representative stress and hardness is assumed,[16]

$$\sigma_r(\varepsilon_r) = C^* \cdot H(\varepsilon_r), \tag{6}$$

with σ_r as the representative stress for a representative strain ε_r and C^* as the constraint factor.

For analytical approaches, as performed in an early work of Prandtl,[15] an equivalent stress has to be defined. Prandtl uses the prominent definition of Tresca and defines the material as rigid-perfectly plastic which finally leads to a constraint factor of 2.57. A later work of Tabor also proposes to use a constant constraint factor C^*, independent of tip angle and material.[16] Indeed, several studies have demonstrated that C^* actually depends on material parameters and tip angle. Literature values for C^* vary between 1 and 3.3 depending on the material. Various approaches showed that with consideration of E/σ_y reasonable C^* values can be determined. Since this ratio is in the same order of magnitude (10^2–10^3) for most conventional metals, a factor of 2.8 as proposed by Tabor is reasonable and will be used throughout this paper.

Similar disagreements still exist in terms of strain definitions. Tabor noted a cotangents dependency of the strain[16,17]:

$$\varepsilon_r = 0.2 \cot(\beta) \tag{7}$$

Definition of strain by Equation 7 will be used in this study. Several other definitions of ε_r emerge in the literature, but are seldom used. Recently, Pathak and Kalidindi tried to describe strain in a more physical way, meaning to relate a length of the unstrained material to the length of the strained material.[6] Even though this was based on the idea of describing the strain introduced by a sphere, one can easily apply Equation 7 to cones. Since those are self-similar, this results in a constant strain, only depending on the cone angle. However, this results in a pre-factor of 0.42 and thereby in far higher strains, but still in a cotangents dependency:

$$\varepsilon_r = \frac{4}{3\pi} \cdot \frac{h_t}{a_c} = \frac{4}{3\pi} \cdot \cot(\beta) \tag{8}$$

Once representative strain and stress are defined, the determination of flow curves is straight forward. Using the four tips with varying apex angle each will provide a data pair of $(\varepsilon_r|\sigma_r)$ for the flow diagram. The additional knowledge of the Young's modulus enables to imprint Hooke's line and will supplement the stress–strain diagram. In the present work, rather than relying on certain assumptions, comparison to known bulk data will justify the correct conversion of stress and strain.

2.6. Hall–Petch Behavior

Since Hall and Petch[31,32] noted the increase of strength with decreasing grain size in mild steel, the HP relation has often been confirmed to describe a broad range of materials and structure sizes. It has also been noted that the HP parameters are dependent on the strain at which the stress values are obtained[33]:

$$H(\varepsilon) = H_0(\varepsilon) + k_{H,HP}(\varepsilon) \cdot \frac{1}{\sqrt{d}} \tag{9}$$

Taking into account the relation between hardness and strength (Eq. 6) for metals, one can simply obtain the stress-related parameter according to

$$\sigma(\varepsilon) = \sigma_0(\varepsilon) + k_{\sigma,HP}(\varepsilon) \cdot \frac{1}{\sqrt{d}} \tag{10}$$

 © 2016 The Authors. Published by WILEY-VCH Verlag GmbH & Co. KGaA, Weinheim

ADVANCED ENGINEERING MATERIALS

The material parameter k_{HP} indicates the extent to which grain boundaries contribute to the strengthening. The higher k_{HP}, the more gain in strength can be reached by the refinement of the microstructure. On the other hand, σ_0 represents the strength of the material in the absence of grain boundaries, which in the end should coincidence with the strength of a single crystal with similar dislocation density ρ. The strength contribution of dislocation hardening may slightly shift the HP-parameters, even though microstructural dimensions of the UFG and NC samples may lead to differing deformation mechanisms, where the $\sim\sqrt{\rho}$ dependency of the flow stress does not necessarily hold true anymore. Moreover, all tips introduce rather large strains and therewith increase the dislocation density around the indent. Naturally, the increase will be higher in single crystals than in the samples with refined microstructure (higher dislocation densities) and reduce the effect on the k_{HP} parameter. Furthermore, it has to be noted that strictly spoken the HP parameters are also influenced by the strain rate of the tests. For fine-grained FCC metals, higher strain-rates will lead to increasing k_{HP} and decreasing σ_0 values, while BCC metals, tested underneath their critical temperature, will show the opposite behavior.

In order to consider hardness measurements of single crystals in the HP analysis, a reasonable grain size has to be chosen. Once the plastic zone size c is significantly smaller than the grain volume, H cannot further be dependent on the grain size. FEM studies of Durst et al. revealed that c is about three times the contact radius a_c when a plastic strain of 0.2% is set as border between plastic zone and unaffected material.[34] This results in a radius of 7–55 μm depending on the used tip. Using Johnsons model, which also includes the mechanical properties if the tested material, c can be predicted by,[13]

$$\left(\frac{c}{a_c}\right)^3 = \frac{1}{3\cdot\tan\beta}\cdot\frac{E}{\sigma_y}, \tag{11}$$

resulting in values of 13–52 μm for Ni and 12–48 μm for W, respectively. These values should be seen as a lower bound but due to the $\propto d^{-\frac{1}{2}}$ relation, and obtained HP parameters are insensitive to the used grain size in this order of magnitude anyway, as the forest dislocation spacing will set the smaller internal length scale. Taking into account the mentioned aspects, mechanical data obtained in this study can be used to extract HP parameters and examine their dependency on strain.

3. Results and Analysis

3.1. Comparison between Vickers and Nanoindentation Hardness

Evaluation of the hardness values for all tested materials shows good agreement between Berkovich nanoindentation and Vickers microhardness tests as demonstrated in Figure 2. However, even after the indicated corrections regarding contact area, there is a slight underestimation of the hardness when microhardness measurements are considered. The misfit, displayed with open triangles in Figure 2, does not exceed 13% and apparently scales with the microstructure size. A difficulty in microhardness measurements is that Vickers tips can commonly not be calibrated and therefore a deviation of the tip angle and consequently the representative strain are not known. Overall, the materials show the expected trend, as hardness clearly increases with decreasing grain size.

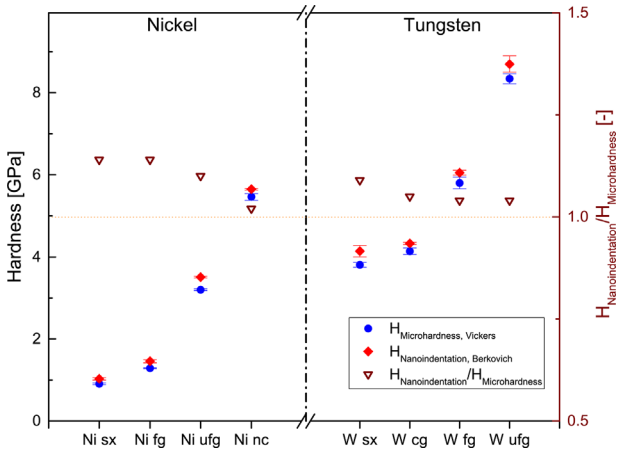

Fig. 2. Comparison between nanoindentation hardness data measured with a Berkovich tip and Vickers microhardness measurements which were corrected according to issues mentioned in Section 2.3. The relative mismatch between the hardness values is illustrated with open triangles.

3.2. Hall–Petch Behavior

Beside the mechanical behavior of the individual samples, the obtained nanoindentation data also allows to determine HP parameters for each tip type, and thereby for varying values of representative strain. Cross-sections of the corresponding cones are shown to scale above the diagram in Figure 3. The correlation coefficient for Ni is 0.961 on average

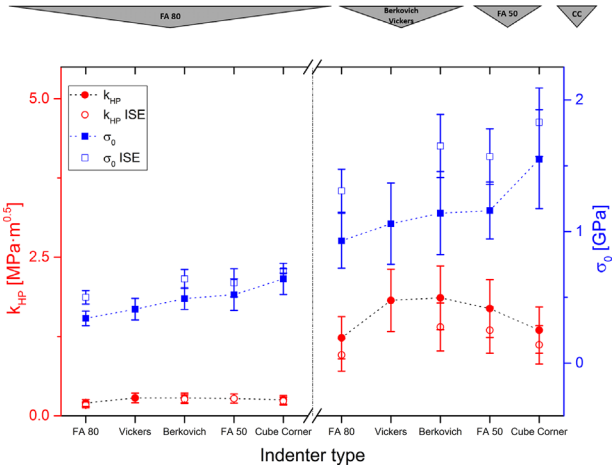

Fig. 3. HP parameter in dependence of the used indenter type. Representative cones of all used tips, imprinted above the diagram to scale. As expected, σ_0 increases with decreasing tip angle. The HP parameter k_{HP} shows a slight increase from FA80 to Berkovich and decreases again for tips with smaller apex angle. Open symbols are referred to data still including the ISE.

and 0.996 for W, suggesting that the HP behavior is valid down to the smallest grain size tested and that the contribution of dislocation hardening is negligible. Figure 3 shows k_{HP} and σ_0 in dependence of the tip type, where error bars were obtained by error analysis using the total differential method. HP parameters naturally vary with strain and are eventually dependent on the hardening behavior of the individual samples. Therefore, coarse-grained metals which are expected to show distinct hardening compared to their fine structured counterparts will exhibit reduced k_{HP} and additionally increased σ_0 at high strains, a trend clearly observed in the present study. The k_{HP} values obtained by ISE corrected data for Ni is in the range between 0.2 and 0.28 MPa m$^{-1/2}$, for W k_{HP} is significantly higher ranging from 1.23 to 1.86 MPa m$^{-1/2}$. The strength of the grain interior given by σ_0 continuously increases with higher strains. If hardness is still affected by the ISE (illustrated as open symbols in Figure 3), this of course rises the level of σ_0. For Ni, the different analysis ends up in the same k_{HP} values, while for W a slight decrease is observed.

3.3. Nanoindentation Flow Curves

The indentation flow curves of the tested samples are displayed in Figure 4. The refinement of the Ni and W microstructure considerably increases the stress levels and leads to a reduced hardening behavior. The hardness values of CG W only slightly deviate from SX W. However, since the volume of the plastic zone introduced by nanoindentation is distinctly smaller than the average grain volume, grain boundaries will only play a minor role and hardly contribute to higher hardness values. For UFG Ni, NC Ni, and UFG W even a slight softening behavior is observable at high strains. The open symbols represent data still including the ISE contribution. Consequently, the stress values especially of coarse microstructures are shifted to significant higher levels, nonetheless the trends in flow behavior remain the same.

4. Discussion

4.1. Microhardness versus Nanoindentation

Only little attention in the literature is paid to proper comparison of hardness data. As demonstrated, one has to be cautious when hardness values from different measurement techniques are compared. At first, it has to be ensured that the used tips have a comparable representative strain, such as Berkovich and Vickers tips. If so, also the analysis procedure has to be carefully reviewed in order to avoid mismatches. In the investigated case of Berkovich nanoindentation and Vickers microhardness testing, neglecting the differences in analysis procedure as described in Section 2.3 would end up in errors up to 30%, while after correcting the error drops to levels below 10% in average. A slight underestimation of microhardness has also been noted in FEM studies on thin films.[35] Riester et al. showed in a study that the nanoindentation hardness values can also be lower if the tip shape differs from specification. Recalculating their tip shapes from calibration data shows a strain deviation of 0.6% between Berkovich and Vickers tip, which consequently leads to higher hardness values for the Vickers measurements.[14] Since the correct shape of the Vickers tip is not known, this remains a potential error source in the current work. A slightly higher apex angle of the Vickers tip would agree well with the findings in this study. Coarse-grained materials, which naturally feature a more distinct work hardening, would then show a larger relative misfit, as observed in this study.

4.2. Hall–Petch Behavior

As demonstrated, HP-constants should carefully be used since there are various influences on their absolute values. Due to the strain dependency, literature values have to be carefully reviewed. Figure 3 demonstrates that a significant difference of HP values, obtained at different strain levels, may occur. This mismatch may even grow if the parameters are obtained by uniaxial tests, where the flow stress at a plastic strain of only 0.2% is used, thus excluding most strain

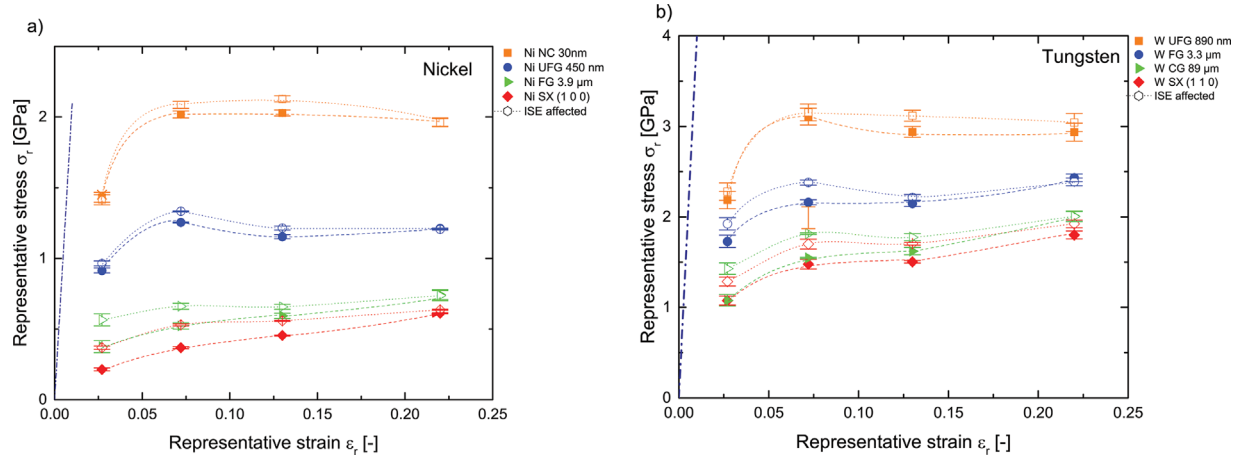

Fig. 4. Indentation flow curves for (a) Ni and (b) W with different microstructures. As expected, coarse grained materials and single crystals show a low yield stress and significant hardening behavior with increasing strain. NC and UFG samples show a slight decrease of stress at higher strains.

 © 2016 The Authors. Published by WILEY-VCH Verlag GmbH & Co. KGaA, Weinheim

hardening contributions. Despite strain and strain-rate dependency, also the dislocation hardening behavior of the tested samples has to be considered. Since σ_0 can be understood as the strength of the grain interior, this value will be influenced by the dislocation densities of the used samples. As seen for Ni in this study, this can still end up in lower stress values for the tested single crystal compared to the σ_0 values. This most likely results from a lower dislocation density of the tested SX compared to the samples with refined microstructures.

Overall, the obtained HP-parameters agree well with literature values ranging from 0.16 to 0.24 MPa $m^{0.5}$.[36–39] Carlton and Ferreira collected literature data and provided a fit of all data, which ends up in an average value of 0.21 MPa $m^{0.5}$.[40] Tungsten is close to literature values as well, even though no comprehensive data could be found in literature. Tests on cold rolled W show values of 0.9 MPa $m^{0.5}$, while samples obtained by powder consolidation exhibited values of around 1.4 MPa $m^{0.5}$[41] (converted to nanoindentation stress following Section 2.3) and are thereby close to values measured in this study. Different to Ni, there is a slight influence on k_{HP} in W when data is not corrected for the ISE.

4.3. Nanoindentation Flow Curves

The slight softening behavior at high strains of the UFG and NC materials has been critically examined. Even though potential analysis errors may result from the constraint factor or occurring pile-ups, as illustrated in Figure 5, these would even lead to even lower hardness values. Moreover, as the stiffness is recorded continuously during indentation and the Young's modulus profiles show the expected values independent of depth (e.g. Figure S1), a strong influence of pile-ups can be excluded, although they are clearly visible for FA 50 and Cube Corner indents. Moreover, stress induced softening is known to occur for NC materials[42] and has also been observed in uniaxial compression tests of NC Ni.[43] For Ni, considering slightly differing grain sizes in the compared studies, values obtained by nanoindentation are in excellent agreement with literature values from uniaxial tests. Figure 6 demonstrates the importance of correcting stress values for the ISE, particularly CG and SX samples. Without that correction stress levels are significantly above values found in literature. Data for high strains as introduced by Cube Corner or FA 50 is lacking in the literature, as in uniaxial tests samples often fail due to poor ductility before reaching such strains. The multiaxial stress state during nanoindentation with a high hydrostatic contribution allows to test at higher strains.

The machining of uniaxial testing samples of W is challenging. This might be the reason for the lack of data literature, which makes it difficult to compare our results. Therefore, mainly Vickers hardness data is presented in Figure 6b, which was corrected the same way as the Vickers values in this study. Taking into account the varying grain sizes, one can see that data of the present study is in good agreement with literature data.

5. Summary and Conclusions

The present study demonstrates that a variety of mechanical properties can be obtained by nanoindentation measurements. Certainly, analysis has to be performed carefully and used parameters have to be reported to feasibly compare data to existing literature. For the comparison of hardness data not only the analysis procedure has to be known, but also tips have to be well calibrated. The actual representative cone angle has by far more validity than the specified angle, when the definitions of ε_r and σ_r proposed by Tabor are used.[16] Further, following conclusions can be drawn:

1) When the standard Berkovich tip is used for nanoindentation, hardness values are in good agreement with conventional Vickers hardness tests (Figure 2). However, a series of corrections has to be applied in the analysis, since

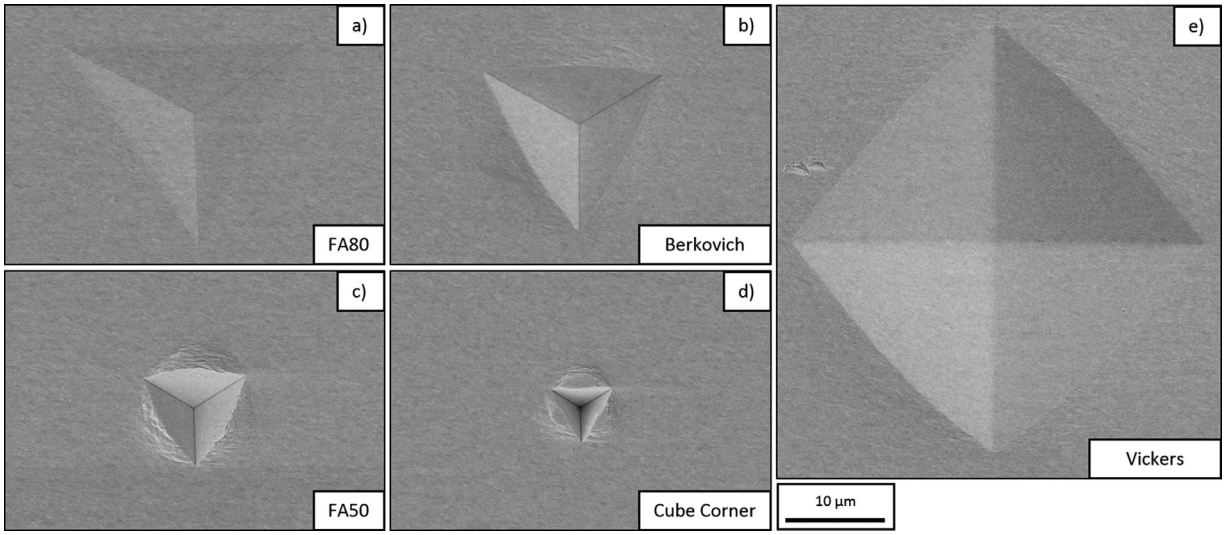

Fig. 5. (a–e) SEM micrographs of residual impressions on UFG Ni for all used tips at the same magnification. With decreasing tip angle, material pile-ups become more distinct.

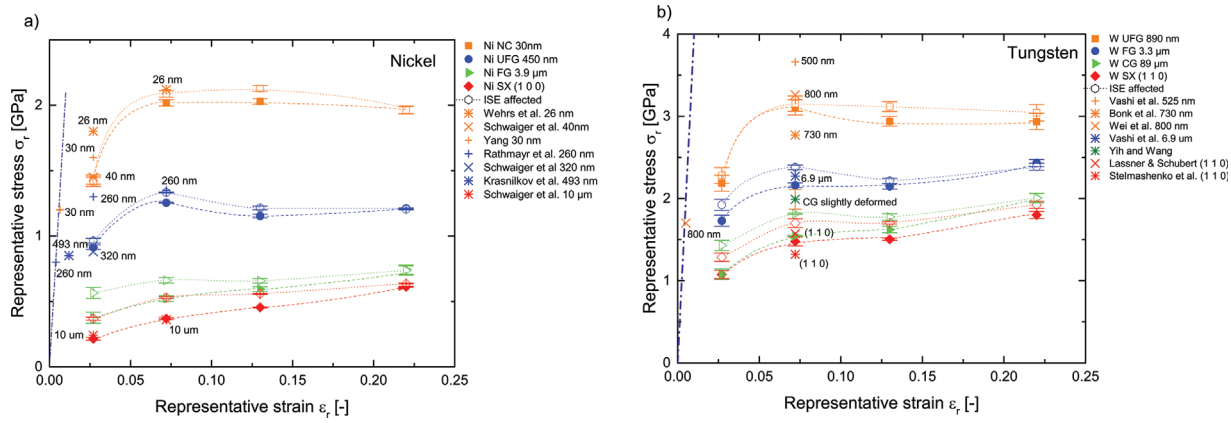

Fig. 6. Comparison of flow stress values obtained in the present study by nanoindentation with literature values from uniaxial tests for (a) Ni[44–48] and (b) W.[41,49–53] The average grain sizes are imprinted at the corresponding symbol.

H is defined differently in these testing techniques. The knowledge of the actual tip shape is crucial since this will affect ε_r and consequently the measured hardness. Deep indentation depths should be favored to avoid influences of tip imperfections.

2) Testing of Ni and W with various grain sizes allows to obtain HP parameter at four different strains. All determined values coincidence well with literature values although those are commonly obtained by uniaxial testing techniques. The profiles of σ_0 and k_{HP} show the expected trends for both materials in dependence of the strain and are slightly sensitive to an occurring indentation size effect.

3) Using an approach with various sharp tips certainly allows to describe the flow behavior of metals, and due to the high hydrostatic component of the stress field even brittle materials can be tested at high strains. By accurate calibration of the tips, local indentation flow curves can be extracted and are in good accordance to literature values of uniaxial tests.

Summarized, nanoindentation is an outstanding technique to extract mechanical properties of metals, especially when material is limited, demanding to machine, or high lateral resolution is required. We clearly demonstrated that HP parameters as well as the flow behavior can be obtained utilizing the multiple sharp tip approach, and results can be evidently compared to data determined by uniaxial experiments. However, the physical background of the strain relation is not yet clarified but future work will be addressed to this topic. Certainly, finite element simulations concerning the influence of tip imperfections would optimally complement the present study will therefore be subject of prospective studies.

Article first published online: November 29, 2016
Manuscript Revised: November 9, 2016
Manuscript Received: September 23, 2016

[1] R. L. Smith, G. E. Sandly, *Proc. Inst. Mech. Eng*. **1922**, *102*, 623.
[2] F. Schulz, H. Hanemann, *Z. Metallkd*. **1941**, *33*, 124.
[3] R. Z. Valiev, Y. Estrin, Z. Horita, T. G. Langdon, M. J. Zehetbauer, Y. T. Zhu, *Mater. Res. Lett*. **2016**, *4*, 1.
[4] W. C. Oliver, G. M. Pharr, *J. Mater. Res*. **1992**, *7*, 1564.
[5] S. Basu, A. Moseson, M. W. Barsoum, *J. Mater. Res*. **2006**, *1*, 2628.
[6] S. Pathak, S. R. Kalidindi, *Mater. Sci. Eng. R*. **2015**, *91*, 1.
[7] S. Shim, J. Jang, G. M. Pharr, *Acta Mater*. **2008**, *56*, 3824.
[8] D. K. Patel, S. R. Kalidindi, *Acta Mater*. **2016**, *112*, 295.
[9] K. Fu, L. Chang, B. Zheng, Y. Tang, H. Wang, *Mater. Des*. **2015**, *65*, 989.
[10] H. Chen, L.-X. Cai, *Acta Mater*. **2016**, *121*, 181.
[11] Y.-T. Cheng, C.-M. Cheng, *Mater. Sci. Eng. R*. **2004**, *44*, 91.
[12] N. Chollacoop, M. Dao, S. Suresh, *Acta Mater*. **2003**, *51*, 3713.
[13] K. L. Johnson, *J. Mech. Phys. Solids* **1970**, *18*, 115.
[14] L. Riester, R. J. Bridge, K. Breder, *MRS Proc. Symp. T*. **1998**, *522*, 45.
[15] L. Prandtl, *Nachr. Gesell. Wissensch. Gött*. **1920**, 74.
[16] D. Tabor, *The Hardness of Metals*, OUP Oxford, Oxford, UK **1951**.
[17] A. G. Atkins, D. Tabor, *J. Mech. Phys. Solids* **1965**, *13*, 149.
[18] S.-D. Mesarovic, N. A. Fleck, *Proc. R. Soc. London Ser. A* **1999**, *455*, 2707.
[19] Y.-T. Cheng, C.-M. Cheng, *Surf. Coat. Technol*. **2000**, *133*, 417.
[20] A. Clausner, F. Richter, *Eur. J. Mech. A Solids* **2015**, *51*, 11.
[21] J. L. Hay, W. C. Oliver, A. Bolshakov, G. M. Pharr, *MRS Proc*. **1998**, *522*, 101.
[22] T.-H. Pham, J. J. Kim, S.-E. Kim, *Int. J. Mech. Sci*. **2015**, *90*, 151.
[23] H. E. Boyer, T. L. Gall, *Metals Handbook*, American Society for Metals, Materials Park, OH, USA **1985**.
[24] T. Leitner, A. Hohenwarter, R. Pippan, *Mater. Sci. Eng. A* **2015**, *646*, 294.

 © 2016 The Authors. Published by WILEY-VCH Verlag GmbH & Co. KGaA, Weinheim

[25] V. Maier, C. Schunk, M. Göken, K. Durst, *Phil. Mag*. **2015**, *95*, 1766.
[26] A. P. Zhilyaev, G. V. Nurislamova, B.-K. Kim, M. D. Baro, J. A. Szpunar, T. G. Langdon, *Acta Mater.* **2003**, *51*, 753.
[27] A. Khorashadizadeh, D. Raabe, M. Winning, R. Pippan, *Adv. Eng. Mater.* **2011**, *13*, 245.
[28] D. B. Bober, A. Khalajhedayati, K. Mukul, T. J. Rupert, *Metall. Mater. Trans. A* **2016**, *47*, 1389.
[29] W. D. Nix, H. Gao, *J. Mech. Phys. Solids* **1998**, *46*, 411.
[30] K. Durst, B. Backes, O. Franke, M. Göken, *Acta Mater.* **2006**, *54*, 2547.
[31] E. O. Hall, *Proc. Phys. Soc. London Sec. B* **1951**, *64*, 747.
[32] N. J. Petch, *J. Iron Steel Inst*. **1953**, *174*, 25.
[33] R. Armstrong, I. Codd, R. M. Douthwaite, N. J. Petch, *Phil. Mag*. **1962**, *7*, 45.
[34] K. Durst, B. Backes, M. Göken, *Scr. Mater.* **2005**, *52*, 1093.
[35] N. A. Sakharova, J. V. Fernandes, J. M. Antunes, M. C. Oliveira, *Int. J. Solids Struct*. **2009**, *46*, 1095.
[36] A. W. Thompson, *Acta Metal*. **1975**, *23*, 1337.
[37] F. Ebrahimi, G. R. Bourne, M. S. Kelly, T. E. Matthews, *Nanostruct. Mater.* **1999**, *11*, 343.
[38] X. Feaugas, H. Haddou, *Metall. Mater. Trans. A* **2003**, *34*, 2329.
[39] A. Godon, J. Creus, S. Cohendoz, E. Conforto, X. Feaugas, P. Girault, C. Savall, *Scri. Mater.* **2010**, *62*, 403.
[40] C. E. Carlton, P. J. Ferreira, *Acta Mater.* **2007**, *55*, 3749.
[41] U. K. Vashi, R. W. Armstrong, G. E. Zima, *Metall. Trans*. **1970**, *1*, 1769.
[42] K. Zhang, J. R. Weertman, J. A. Eastman, *Appl. Phys. Lett*. **2005**, *87*, 061921.
[43] W. Blum, Y. J. Li, *Scr. Mater.* **2007**, *57*, 429.
[44] J. Wehrs, G. Mohanty, G. Guillonneau, A. A. Taylor, X. Maeder, D. Frey, L. Philippe, S. Mischler, J. M. Wheeler, J. Michler, *JOM* **2015**, *67*, 1684.
[45] R. Schwaiger, B. Moser, M. Dao, N. Chollacoop, S. Suresh, *Acta Mater.* **2003**, *51*, 5159.
[46] N. Krasilnikov, W. Lojkowski, Z. Pakiela, R. Valiev. *Mater. Sci. Eng. A* **2005**, *397*, 330.
[47] B. Yang, PhD thesis, Universität des Saarlandes, 66041 Saarbrücken, **2006**.
[48] G. B. Rathmayr, A. Hohenwarter, R. Pippan, *Mater. Sci. Eng. A* **2013**, *560*, 224.
[49] S. W. H. Yih, C. T. Wang, *Tungsten: Sources, Metallurgy, Properties, and Applications*, Plenum Publishing Corporation, New York, NY, USA **1979**.
[50] N. A. Stelmashenko, M. G. Walls, L. M. Brown, Y. V. Milman, *Acta Metall*. **1993**, *41*, 2855.
[51] E. Lassner, W.-D. Schubert, *Tungsten: Properties, Chemistry, Technology of the Element, Alloys, and Chemical Compounds*, Plenum Publishers, New York **1999**.
[52] Q. Wei, L. J. Kecskes, *Mater. Sci. Eng. A* **2008**, *491*, 62.
[53] S. Bonk, J. Reiser, J. Hoffmann, A. Hoffmann, *Int. J. Refract. Met. Hard Mater* **2016**, *60*, 92.